IOP Publishing Journal of Physics D: Applied Physics
J. Phys. D: Appl. Phys. **50** (2017) 395502 (8pp) https://doi.org/10.1088/1361-6463/aa84f7

Thermoelectric figure of merit of polymeric systems for low-power generators

Luigi Cigarini[1,2], Alice Ruini[1,2], Alessandra Catellani[2] and Arrigo Calzolari[2]

[1] Dipartimento di Scienze Fisiche, Informatiche e Matematiche, Università di Modena e Reggio Emilia, Via Campi 213/a, 41125 Modena, Italy
[2] CNR-NANO Research Center S3, Via Campi 213/a, 41125 Modena, Italy

E-mail: arrigo.calzolari@nano.cnr.it

Received 19 May 2017, revised 3 August 2017
Accepted for publication 8 August 2017
Published 11 September 2017

Abstract

The request of thermoelectric materials for low-power and flexible applications fosters the investigation of the intrinsic electron and thermal transport of conducting polymeric chains, which are building blocks of the complex variety of organic composites proposed in experimental samples. Using calculations from first principles and the Landauer approach for both electron and phonon carriers, we study the thermoelectric figure of merit zT of three representative and largely used polymer chains, namely poly(3,4-ethylenedioxythiophene), polyaniline and polyfluorene. Our results provide an upper-limit estimate of zT, due to the intrinsic electronic and vibrational properties of the selected compounds, and pave the way to a microscopic understanding of the mechanisms that affect their electronic and transport characteristics in terms of structural distortions and chemical doping.

Keywords: transport, phonon, organic thermoelectric, density functional theory, DFT, polymer, polymers

(Some figures may appear in colour only in the online journal)

1. Introduction

Sources of renewable energy are a major global concern for researchers. The goal to reduce our energetic dependency from fossile fuels is attracting an ever-increasing attention of the scientific community. Thermoelectricity (TE) plays a prominent role in such scenario, as the Seebeck effect can be used to convert a temperature gradient into an electrical potential [1].

Thermoelectric generators (TEG) are solid-state devices that contain no moving parts and thus can operate over a long period of time without significant maintenance. Small heat sources and limited temperature differences are sufficient to drive thermoelectric generators, which make these devices interesting for applications where traditional dynamic heat engines cannot be employed [2]. TEG produce no vibrations and are highly scalable, they do not use working fluids (e.g. refrigerators), and are expected to produce negligible direct emissions of greenhouse gases [3].

The conversion performance of a TE device is determined by the materials used, the efficiency of which is generally expressed by the figure of merit: $zT = \sigma_{\mathrm{el}} S^2 T/\kappa_t$, where S is the Seebeck coefficient, σ_{el} is the electrical conductivity, κ_t is the thermal conductivity and T is the absolute temperature. The total thermal conductivity is in its turn given by $\kappa_t = \kappa_{\mathrm{el}} + \kappa_{\mathrm{ph}}$, i. e. the sum of an electronic contribution plus a phononic one, related to lattice vibrations.

Traditionally employed inorganic TE materials (ITE) are solid alloys, with both n-type (e.g. Bi_2Te_3, PbTe, $CoSb_3$) and p-type (e.g. Sb_2Te_3, $CeFe_4Sb_{12}$, $Yb_{14}MnSb_{11}$) character and complex crystalline structures (e.g. skutterudites, half-Heusler ceramics, layered lamellae, clathrates, etc) [4]. In principle, TE materials can be put in use in various energy conversion applications ranging from large scale waste heat recovery (e.g. transportation vehicles) to microelectronic (e.g. CPU coolers, GPS) and biomedical devices (e.g. pacemakers), encompassing ten orders of magnitude in power generation from 10 kW to 1 μW. In practice, the commercial application of current ITE materials as high power TEG is strongly hindered by their reduced efficiencies ($zT \sim 1$) [5], together with their intrinsic properties, such as rareness and high cost; therefore, ITEs are still inadequate to compete with

conventional devices based on combustion or thermodynamic processes. On the other hand, their high working temperatures (500–1000 K), their high production cost, and unconvenient mechanical properties, such as hardness and heaviness, make them unfit for low power and flexible TEGs, as required for instance for biomedical sensors, wearable/biocompatible devices [6], or solar TEGs [7].

In contrast, organic thermoelectric materials (OTE) can be readily shaped in a wide range of thin-film and bulk architectures and offer an interesting alternative as plastic renewable energy generators for wireless sensor networks and portable electronics (e.g. wrist watches) [8], which require low power and low temperature ($T \lesssim 300$ K) generators [9–12]. OTEs are based on abundant elements (mostly C, N, O), and their simple structure and composition can be easily optimized with standard chemical synthesis techniques. Compared with the inorganic counterparts, the organic thermoelectric materials are potentially light-weight, flexible, solution-processable, and low-cost. The most employed OTE materials are based on conjugated conducting polymers [13], like polyanilines (PANI) [14–18], polypyrroles (PPY) [19], polycarbazoles (PC) [20], polythiophenes (PTH) [21], poly(3,4-ethylenedioxythiophene) (PEDOT) [22–26].

To maximize TE efficiency, a large Seebeck coefficient, high electrical conductivity, and a low thermal conductivity are required [1]. Unfortunately, increasing S generally results in decreasing σ_{el} [27], while increasing σ_{el} increases κ_{el} (Wiedemann–Franz law). As these transport characteristics depend on interrelated material properties, a number of chemical, structural and electronic parameters need to be optimized to maximize zT. Despite the intrinsic poor thermal transport properties and good Seebeck coefficients [15, 28, 29] electrical conductivity of OTE materials is unfortunately much lower than ITE. Although, acting on doping procedures (e.g. PEDOT:PSS [22]) allows to improve the electrical conductivity [14, 17, 21, 24, 28] of semiconducting polymers, the zT values of these systems are generally largely below 0.5 [11, 30].

Furthermore, the transport characteristics and zT values reported so far show extremely wide ranges of variability covering several order of magnitudes, even for the most studied polymeric systems (e.g. PANI, PEDOT) [30]. For example, in the case of PANI the measured range for the electrical conductivity is $[10^{-7}$–$10^{2}]$ S cm^{-1}, the Seebeck coefficient varies from -16 to 225 μV K^{-1} and κ_t is between 0.02 and 0.54 W mK^{-1} [3]. With a so large variability in the results it is difficult to discriminate the main factors that affect the TE properties of these materials and thereby optimize the conversion process. The discrepancies in these results are usually associated to the details of the chemical synthesis, environmental factors (e.g. temperature, humidity), structural arrangements and doping conditions.

From the theoretical side, while modeling of electronic transport has been extensively tackled [31–34] also in the framework of TE applications [35, 36], much less work was devoted to thermal transport modeling. The phonon transport contribution to zT in organic materials was generally accounted for by using semi-classical approaches, such as the deformation potential approximation [31] or Langevin-type dynamics schemes to model the phonon assisted hole hopping [37]. If such approaches are capable to catch the average dissipative effects in complex polymeric structures, they lack in describing the relationship between chemical/geometrical structure and transport properties of low-dimensional systems. In fact, many atomic-scale effects may strongly impact the intra- or inter-chain transport, such as structural or conformational modifications of the polymeric chain due to folding effects, presence of dopants and counterions, or intentional insertion of lateral moieties [11, 18, 21, 25, 26] On the other hand, a fully quantum-mechanical description of phonon transport in molecular systems is a huge computational challenge, and very few examples have appeared so far [38].

Here we present a first principles investigation of the zT characteristic of prototypical polymer systems, namely PANI, PEDOT and polyfluorene (PFO). PEDOT and PANI are the most studied systems in this field, having, on average, the best zT values measured for p-type organic materials [11, 39]). Although pure PFO (i.e. without co-polymer modifications) is not commonly used as TE materials, here it is considered because of the almost unique opportunity to deal with an organic n-type conductor [40]. PFO is also a very well known system, largely studied for its optoelectronic characteristics. This allows us to have a comprehensive set of materials with different but comparable properties. Both electron and thermal transport characteristics are evaluated at the same level of accuracy, by means of a unified *ab initio* approach, based on the direct calculation of the electronic and vibrational structure of the polymers, resulting from density functional theory simulations.

The target polymers are modeled here as isolated and periodic chains, in order to get a well-established knowledge basis for the electronic and transport properties of the constituent OTE materials. This goal is especially critical for conjugated polymers, since the actual morphology of the film is very rarely known in depth, and usually materials characterized by different morphologies are grouped under the same denomination. A key-role in governing the actual structure in most polymers is played by side chains, whose presence facilitates casting, because they dissolve more easily in a proper wet-chemistry processing. However, side chains typically lead to a very disordered amorphous final configuration, with each conjugated segment either electronically isolated from the neighbors or at most with residual π-coupled segments. In other cases, depending of the growth technique, polymers may aggregate in very compact crystallites in herringbone (HB) or ordered π-stacked configurations, which are typically immersed in amorphous regions. This complexity prevents a unique definition of the structural model that is at the basis of each atomistic DFT calculation. In order to unravel this problem, here we focus on the transport properties of single chains, without chemical dopants. Despite such a crude simplification, this allows us to identify the intrinsic transport properties of the selected polymers and to reveal the mechanisms that affect the large zT variability reported in the experiments.

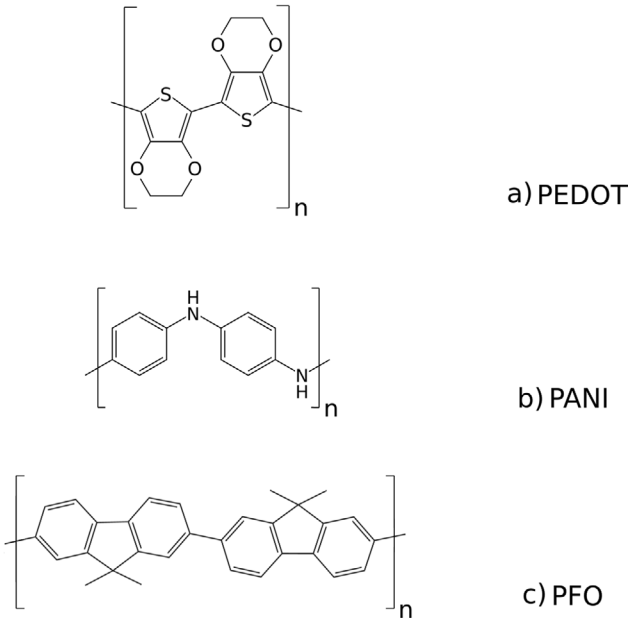

Figure 1. Molecular Structure of (a) PEDOT, (b) PANI and (c) PFO. Each simulation cell contains two monomeric units.

2. Method

All calculations are performed by adopting the planewave formulation of density functional theory (DFT), as implemented in the Quantum ESPRESSO (QE) suite of codes [41]. The exchange-correlation functional is treated within the generalized gradient approximation (GGA) in the form of Perdew–Burke–Ernzerhof (PBE) type parametrization [42], and the Grimme-D2 [43] correction is used to model Van der Waals interactions. Ion potentials are described by *ab initio* ultrasoft pseudopotentials of the Vandebilt's type [44]. The kinetic energy cutoff for planewave expansion of single-particle wavefunctions and charge density is set to 35.0 Ry and 700.0 Ry, respectively. The one dimensional Brillouin zone is sampled using 8 k-points along the chain direction. The structural relaxation was obtained by setting the convergence threshold for forces on all atoms to 3×10^{-7} eV Å^{-1}.

In order to obtain the electronic and thermal coherent transport characteristics, we adopted the WanT package [45], where the Landauer theory based on Green's functions [32, 46] is implemented in a real-space and unified footing for both electron [47] and phonon [48] carriers. A pseudo-atomic projection procedure [49, 50] was performed on top of DFT calculations to obtain the real-space electronic hamiltonian, while phonon spectra and interatomic force constant (IFC) matrices were obtained by means of a finite-differences/finite-fields approach [51], implemented in the Quantum ESPRESSO package as well. IR spectra were calculated according to [52] and [53].

3. Results and discussion

As a first step, we performed a geometrical optimization of the atomic coordinates for the target polymers—simulated as infinite, isolated chains—to then proceed with the calculations of their ground-state electronic structure.

The theoretical pitch of the periodic chains has been obtained by minimizing the total energy of the system, as a function of the cell dimension in the direction along the polymer (see figure 1). The resulting cell parameters are 7.865 Å for PEDOT, 10.313 Å for PANI and 16.786 Å for PFO. The three optimized structures are characterized by an alternating rotation of the monomeric units, around the polymer axis: PEDOT has an almost planar structure, with a torsion angle between monomers very close to 180°, while the torsion angle is slightly smaller for PFO(148.4°) and PANI (155.4°).

The electronic band structures (figure 2) display the typical behaviour of semiconductor systems, with the Fermi level located in the bandgap; the Perdew–Burke–Ernzerhof (PBE-DFT) [42] energy gap amounts to 0.92 eV for PEDOT, 2.36 eV for PANI and 2.17 eV for PFO, while the corresponding band dispersion for the highest occupied electronic bands are 1.62 eV, 1.05 eV and 0.58 eV, respectively, in agreement with previous results [57–59]. Since PFO is generally n-doped, we also report the dispersion of the lowest unoccupied band, which is 0.59 eV.

As a crosscheck test on the structure and composition of polymer models, we compared the experimental and theoretical infrared (IR) spectra, as shown in figure 3. In all three cases, we found a very good theoretical/experimental agreement both on the frequency positions of the main peaks and on assignment of the vibrational modes. Spectra are dominated by a multistructured branch between 1200–1500 cm^{-1} associated to ring stretching and breathing modes. Lower energy peaks in the PEDOT spectra are due to C–S modes, while alkyl C-H rocking modes are responsible for the peak at 820 cm^{-1} in the case of PFO. High frequency C–H stretching modes characterize the range 2855–3100 cm^{-1} of the three systems. The good agreement with the experimental results confirms that, despite the complexity and the disorder of the experimental systems, our models catch all the most relevant phonon features that is the prerequisite for the evaluation of heat transport properties.

Single polymeric chains can be envisaged as quasi one dimensional nanostructures with extremely high surface-to-volume ratio, in the limit of lateral width that tends to zero. In this regime, elastic scattering contributions with the lateral boundaries or geometrical distortions are the predominant causes that affect both electron and thermal transport [60–62]. Thus, the coherent regime is a good first approximation for the description of transport in a large range of temperature, almost up to room temperature. For higher temperatures, transport becomes rather diffusive and dissipative scattering terms (e.g. el–el, el–ph, ph–ph) should be carefully included.

The complete energy band structures and phonon dispersions are exploited to solve an extended Landauer problem by means of the calculation intrinsic coherent transport properties along the polymer chains for both electron and thermal carriers. In other words, the transport properties (e.g. quantum conductance, Seebeck coefficients) are directly linked to the atomistic structure of the system. In fact, all parameters entering the TE

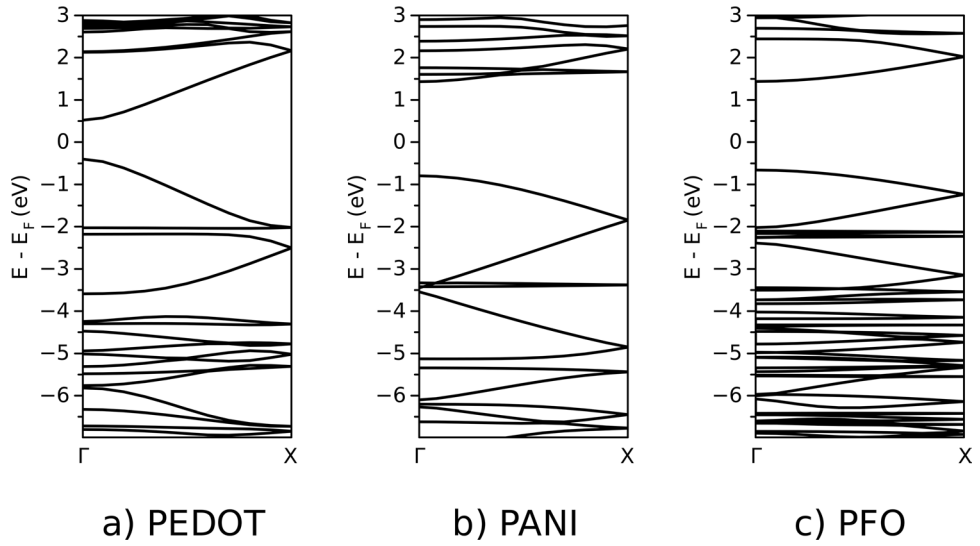

Figure 2. Electronic band structures for the three investigated polymers along the chain direction. The zero of the energy scale is set to the Fermi energy value. (a) PEDOT, (b) PANI and (c) PFO.

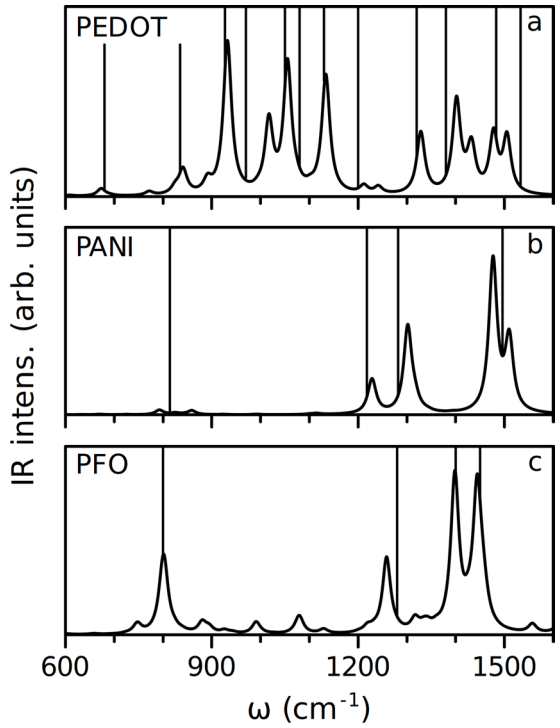

Figure 3. Calculated vibrational spectra for the three investigated polymers. The experimental absorption frequencies are taken from IR spectra and reported as vertical lines for PEDOT [54] in panel (a), for PANI [55] in (b) and for PFO [56] in (c).

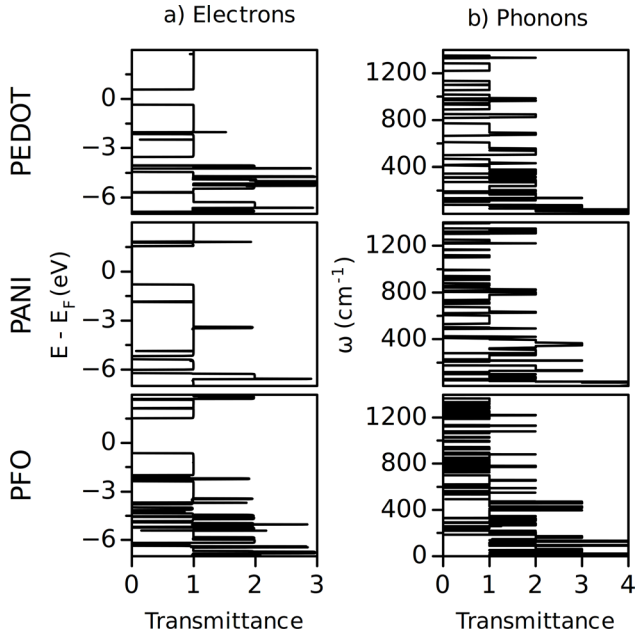

Figure 4. Calculated (a) electronic and (b) phonon energy-dependent transmission functions for PEDOT, PANI and PFO.

figure of merit are calculated in the Landauer framework from the energy-dependent transmission functions for electrons ($\mathcal{T}_{\rm el}$) and phonons ($\mathcal{T}_{\rm ph}$). The electronic part can be straightforwardly obtained from a tight-binding-like Hamiltonian matrix [47, 50] that results from a real-space transform of the corresponding plane-wave one, as calculated from the DFT cycle. The calculation of IFC matrices, needed for the phonon transmission function, are obtained from a direct finite-differences (FD) approach, which results to be computationally more efficient than standard density functional perturbation theory (DFPT) approaches [63], for low-symmetry systems like the ones under consideration. In order to take into account long-range interactions that are important for the low-frequency wavevectors contributions to phonons (i.e. $q \to 0$), we adopted a supercell approach. For each system, we considered a four-fold orthorombic supercell, including four replicas of the original unit cell along the polymer direction, and we calculated forces (i.e. IFC) displacing only the atoms in the primitive cell back and forth along the three spatial directions. This corresponds to a set of $6 \times N$ DFT calculations, where N is the number of atoms in the original cell (see figure 1). The complete IFC is then recovered, by applying translational symmetry operations [48].

Figure 4 summarizes the calculated transmission functions for (a) electron and (b) phonon carriers. All the spectra have a step-like behavior typical of periodic systems. In the absence

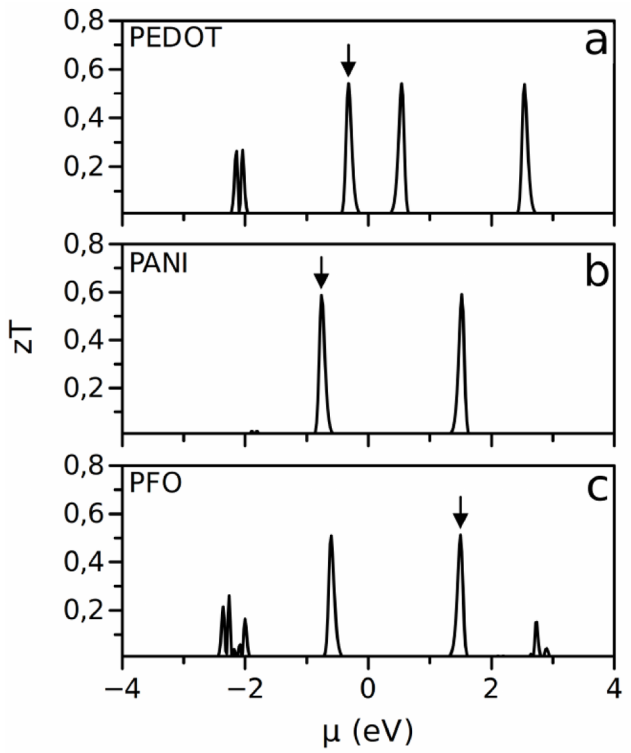

Figure 5. zT values, obtained as functions of the chemical potential at 300 K for PEDOT, PANI and PFO. Zero energy reference for each system is set to the Fermi level of the corresponding undoped system. Vertical arrows mark the peak values reported in table 1, and discussed in the text.

of external leads, at a given value of energy (wavenumber), the quantum transmittance is constant and proportional to the number of transmitting channels available for charge (phonon) mobility, which are equal to the number of conducting bands at the same energy. In the energy range close to the Fermi energy the value of $\mathcal{T}_{el}$ is one (in unit of $2e^2/h$) for both electron and holes for the three systems: this derives from the unique single-degenerate band that characterizes the maximum of the valence band and the minimum of the conduction band in this kind of systems. Such low number of channels available for charge transport explains the origin of the intrinsic low electron conductivity in these polymeric structures.

Phonon transmission functions also assume low values (1–2 unit of $\pi^2 k_B^2 T/(3h)$) in the low energy range, which is the one that mainly contributes to coherent phonon conductivity. This is in agreement with low thermal conductivity measured in the experiments, and is one of the main desired requisites for TE applications. In particular, $\mathcal{T}_{ph}$ has its maximum value (four quanta of transmittance) at zero frequency, which accounts for the four acoustic modes (three spatial translations and one rotation around the polymer axis), that are shifted to zero energy at Γ point by the application of the one-dimension acoustic sum rule. In 3D systems, the spatial hindrance due to polymer assembly inhibits the rotational degree of freedom of the single chain, further reducing the contribution of acoustic phonons to $\mathcal{T}_{ph}$ at low energy [48].

In the coherent transport approximation, i.e. in the absence of inelastic scattering processes, the figure of merit reduces to: $ZT = S^2 G_{el} T/K_t$ [64], where G_{el} and $K_t = K_{el} + K_{ph}$ are the corresponding quantum conductance terms. G_{el}, K_{el} and S can be derived from the electronic transmission $\mathcal{T}_{el}$ by defining an intermediate function $L_n(\mu, T)$ of the chemical potential (μ) and the temperature [65]:

$$L_n(\mu, T) = \frac{2}{h} \int \mathrm{d}E \mathcal{T}_{el}(E-\mu)^n \left[\frac{\partial f(E,\mu,T)}{\partial E}\right]. \quad (1)$$

By using the standard kinetic relations we obtain:

$$G_{el} = \frac{2e^2}{h}\mathcal{T}_{el}(\mu) = e^2 L_0(\mu, T), \quad (2)$$

$$K_{el}(\mu, T) = \frac{1}{T}\left[L_2(\mu, T) - \frac{L_1(\mu, T)^2}{L_0(\mu, T)}\right], \quad (3)$$

$$S(\mu, T) = \frac{1}{qT}\left[\frac{L_1(\mu, T)}{L_0(\mu, T)}\right]. \quad (4)$$

The phonon thermal conductance K_{ph} can be obtained from $\mathcal{T}_{ph}$ via direct integration:

$$K_{ph}(T) = \frac{1}{2\pi\hbar}\int_0^\infty d(\hbar\omega)\mathcal{T}_{ph}(\omega)\hbar\omega\left[\frac{\partial n(T,\omega)}{\partial T}\right], \quad (5)$$

where $n(T, \omega)$ is the Boltzman distribution for bosons at temperature T.

The resulting zT values, obtained as functions of the chemical potential at 300 K, are reported in figure 5, while the behavior of the Seebeck coefficient and electronic conductance wrt μ are shown in figure 6. Doping effects were then introduced by shifting the Fermi level (i.e. the chemical potential) across the bandstructure, i.e. within the rigid-band approximation. Zero energy reference for each system is set to the Fermi level of the undoped system, which lies in the middle of the bandgap. Positive μ values correspond to n-type doping (i.e. Fermi level in the conduction band), while negative values correspond to p-type doping (i.e. Fermi level in the valence band). In table 1, we focus on the zT peaks in the proximity of the bandgap corresponding to lowest chemical potential (vertical arrows in figure 5) associated to the specific p-type (n-type) doping character, usually assumed in experimental samples by PEDOT and PANI (PFO), respectively.

From the analysis of zT it results that: (i) the calculated values for S and K_{ph} are in good agreement with most experimental measurements [11, 30]. In correspondence to the principal peaks in the zT function, the Seebeck coefficient of PFO and PANI ($S > 2.4$ μV K^{-1}) has a higher absolute value for the Seebeck coefficient than PEDOT ($S < 2$ μV K^{-1}). (ii) In the case of PEDOT the lowest energy peak corresponds to small value of chemical potential, which means that low doping level and/or small applied electric field ($\mu = -0.34$ eV) are sufficient to have TE conversion. On the contrary PANI and PFO require higher applied chemical potentials (-0.76 eV and $+1.50$ eV, respectively). This trend correlates with the energy gap and band dispersion of the single polymers discussed above. (iii) At the selected values of the chemical potential, the three polymres have very similar zT values. This derives from the fact that, despite the lateral chemical decorations, the three systems have a similar (simple) structure based on the similar conjugated sequences of carbon rings. On the

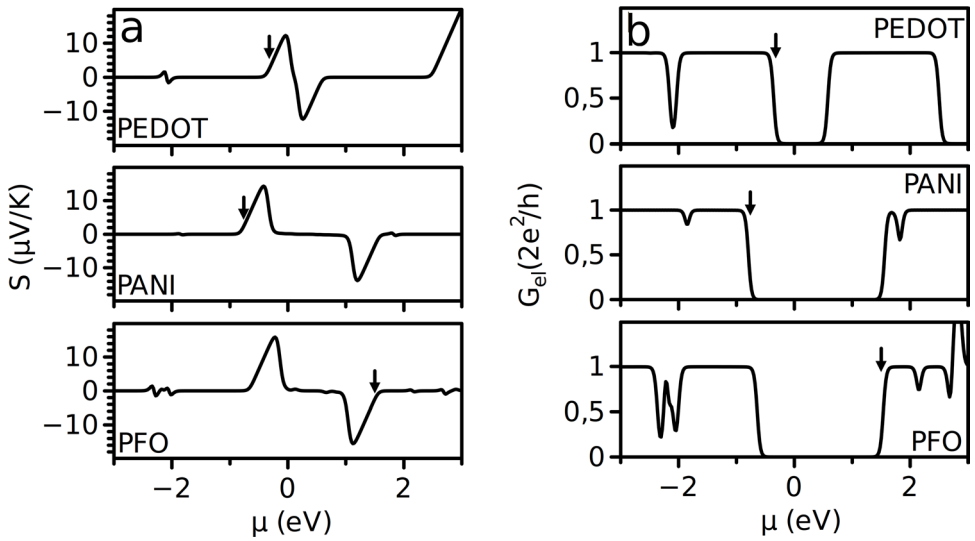

Figure 6. Calculated (a) Seebeck coefficient and (b) electronic conductance as functions of the chemical potential at 300 K for the three polymers: PEDOT, PANI and PFO. Vertical arrows mark, in the potential energy scale, the positions of the zT functions peak values reported in table 1, in figure 5 and discussed in the text.

other hand, the resulting zT value for PANI (0.57) is slightly higher than PEDOT's one (0.55), in contrast with the general experimental trends that show highest zT values for PEDOT ($zT = 0.42$). This discrepancy is not dramatic as both values are well within the variability range reported in the experimental measurements [11, 30]; and may be due to specific structural, doping and environmental conditions. (iv) In general, the theoretical value that we obtain for the single chains are overestimated with respect to the experimental values. The calculated zT values reported here can be considered as theoretical upper-limit values for real systems, since they include intrinsic properties of the ideal materials. In general, structural disorder, defects and impurities, temperature effects and dissipative scattering processes (e.g. el-ph, ph-ph) are known to be detrimental for the TE conversion efficiency of organic materials. However, a clear distinction between electron and phonon carriers can be drawn. On the basis of the comparison with the IR spectra presented above, we can conclude that even this simple chain model is representative of most of the vibrational properties of the system. This is probably due to the fact that the low thermal transport in these materials is due to the strong (i.e. rigid) character of the C–C bonds that form the backbone of all these polymeric structures. Standard out-of-plane torsion angle between C-rings along the chains are typically associated to small frequency deviations (few cm^{-1}) of the phonon modes, while 3D stacking and/or chain distortions are relevant on higher length scale that do not remarkably affect the vibrational properties of the single polymers. The combination of these effects may actually reduce the intrinsically low thermal conductivity of the compound.

Concerning electron carriers, we already mentioned that all these polymers have only one single band (close to the bandgap) available for transport along the chain. In contrast with the phonon counterpart, electron transport is much more sensitive to internal inter-ring torsional distortions or to the presence of defects, because even small deviations from the ideal geometry correspond to a reduction

Table 1. Peak values of zT as a function of the chemical potential (μ) for the three polymers. The quantities of interest in the calculation of zT, at the same chemical potentials of peak zT values, are also reported, namely electrical conductance G, Seebeck coefficient S, electronic k_{el} and phononic thermal conductance k_{ph}. All the values are calculated at $T = 300K$.

	zT	S (μV K^{-1})	G (S)	K_{el} (nW K^{-1})	K_{ph} (nW K^{-1})
PEDOT ($\mu = -0.34$ eV)	0.55	1.88	0.221	0.070	0.358
PANI ($\mu = -0.76$ eV)	0.57	2.41	0.119	0.042	0.321
PFO ($\mu = 1.50$ eV)	0.51	−2.45	0.118	0.040	0.376

of the electron conjugation along the polymer as well as a shrinking and/or a flattening of the energy bands (i.e. net reduction of the electron mobility) [13, 62, 66]. This results in an easy deterioration of an intrinsic low electrical conductivity. Doping may shift the position of the Fermi level in the polymer bands, but it is not able to really increase the density of states (i.e. the conductivity) of the sample. In this regard, such a simple 1D electronic structure (e.g. one conductive band) constitutes a basic limitation in the possibility of improving the conductivity of the sample. In fact, this does not allow for an advanced bandstructure manipulation as it happens, for example, in multipocket conductors such as partially filled skutterudites [67]. On the other hand, other charge transfer mechanisms [68], such as intra- and inter-chain hopping, are not efficient enough to assure high electron conductivities.

Doping processes deserve a separate comment. From table 1 we note that a remarkable zT value also for PFO, which, instead, is not usually used as TE materials. While PEDOT and PANI may be easily p-doped through oxidative processes, which add electron acceptor moieties without changing to the existing polymer skeleton (e.g. in PEDOT:PSS [69, 70],

PANI:CSA [11]), the high oxidative stability of PFO, which is the key property for its optoelectronic applications, prevents this simple doping procedure. In order to change the electronic properties of PFO it is generally necessary to include co-polymer units along the conjugated chain, i.e. changing the intrinsic nature of PFO. Furthermore, with respect to PEDOT and PANI, electron transport in PFO is plagued by an higher level of intrinsic charge traps in the gap [71], which degrade its electron conductivity [72]. However, if native PFO is not considered as a TE material, other PFO-derivatives [73], or structurally similar polymeric systems (e.g. polyphenylene [74] and polycarbazole [20]) are assuming increasing interest in TE applications, in particular in connection with other nanostructured composites.

4. Conclusions

We presented a fully *ab initio* study of the TE characteristics of organic polymeric systems. Our results indicate qualitative similarities among the three studied polymers, namely PEDOT, PANI and PFO, when considered in their ideal and isolated configuration and define an upper-limit estimate of the zT figure of merit, in qualitative agreement with most experimental results. This determines the main intrinsic TE properties of original conducting polymers, which is the necessary prerequisite to understand the TE response of the corresponding experimental systems, where the complex interplay between structural disorder, environmental conditions and dissipative scattering effects prevents a simple interpretation of the experimental results, as demonstrated by the large variability of the data reported so far. The choice of a simplified, albeit controlled model system, along with a microscopic approach, allowed us to discriminate the main mechanisms that affect both the electronic and thermal transport along polymers at the same level of accuracy, unraveling the interplay between chemical structure and thermoelectric properties of the constituent polymer chains. This is particularly true for the thermal transport contribution that is rarely considered in theoretical investigation, as it requires the quantum mechanical modelling of the entire phonon structure.

Acknowledgments

We acknowledge the CINECA award under the ISCRA initiative (project IsC34_OrgTE), for the availability of high performance computing resources and support.

ORCID iDs

Luigi Cigarini https://orcid.org/0000-0003-1898-985X

References

[1] Goldsmid H J 2016 *Introduction to Thermoelectricity* (Berlin: Springer)
[2] Alam H and Ramakrishna S 2013 *Nano Energy* **2** 190
[3] Elsheikh M H, Shnawah D A, Sabri M F M, Said S B M, Hassan M H, Bashir M B A and Mohamad M 2014 *Renew. Sustain. Energy Rev.* **30** 337
[4] Gaultois M W, Sparks T D, Borg C K H, Seshadri R, Bonificio W D and Clarke D R 2013 *Chem. Mater.* **25** 2911
[5] Snyder G J and Toberer E S 2008 *Nat. Mater.* **7** 105
[6] Park T, Park C, Kim B, Shin H and Kim E 2013 *Energy Environ. Sci.* **6** 788
[7] Lee J, Yoo D, Park C, Choi H and Kim J 2016 *Solar Energy* **134** 479
[8] Siddique A R M, Mahmud S and Van Heyst B 2017 *Renew. Sustain. Energy Rev.* **73** 730
[9] Bubnova O and Crispin X 2012 *Energy Environ. Sci.* **5** 9345
[10] Chen Y, Zhao Y and Liang Z 2015 *Energy Environ. Sci.* **8** 401
[11] Du Y, Shen S Z, Cai K and Casey P S 2012 *Prog. Pol. Sci.* **37** 820
[12] He M, Qiu F and Lin Z 2013 *Energy Environ. Sci.* **6** 1352
[13] Peng S, Wang D, Lu J, He M, Xu C, Li Y and Zhu S 2017 *J. Pol. Environ.* 1
[14] Li J, Tang X, Li H, Yan Y and Zhang Q 2010 *Synth. Met.* **160** 1153
[15] Yan H, Sada N and Toshima N 2002 *J. Therm. Anal. Cal.* **69** 881
[16] Sun Y, Wei Z, Xu W and Zhu D 2010 *Synth. Met.* **160** 2371
[17] Jin J, Wang Q and Haque M A 2010 *J. Phys. D.: Appl. Phys.* **43** 205302
[18] Cho C, Stevens B, Hsu J-H, Bureau R, Hagen D A, Regev O, Yu C and Grunlan J C 2015 *Adv. Mater.* **27** 2996
[19] Zhang Z, Chen G, Wang H and Zhai W 2015 *J. Mater. Chem.* C **3** 1649
[20] Levesque I *et al* 2007 *Chem. Mater.* **19** 2128
[21] Endro B, Mellar J, Gingl Z, Visy C and Janaky C 2015 *J. Phys. Chem.* C **119** 8472
[22] Kim G-H, Shao L, Zhang K and Pipe K P 2013 *Nat. Mater.* **12** 719
[23] Yue R and Xu J 2012 *Synth. Met.* **162** 912
[24] Bubnova O, Khan Z U, Malti A, Braun S, Fahlman M, Berggren M and Crispin X 2011 *Nat. Mater.* **10** 429
[25] Yoo D, Kim J, Lee S H, Cho W, Choi H H, Kim F S and Kim J H 2015 *J. Mater. Chem.* A **3** 6526
[26] Zhang B, Sun J, Katz H E, Fang F and Opila R L 2010 *ACS Appl. Mater. Inter.* **2** 3170
[27] Mateeva N, Niculescu H, Schlenoff J and Testardi L 1998 *J. Appl. Phys.* **83** 3111
[28] Bubnova O *et al* 2014 *Nat. Mater.* **13** 190
[29] Lu N, Li L and Liu M 2015 *Phys. Rev.* B **91** 195205
[30] Kroon R, Mengistie D A, Kiefer D, Hynynen J, Ryan J D, Yu L and Müller C 2016 *Chem. Soc. Rev.* **45** 6147
[31] Chen J, Wang D and Shuai Z 2012 *J. Chem. Theo. Comput.* **8** 3338
[32] Buongiorno Nardelli M 1999 *Phys. Rev.* B **60** 7828
[33] Samanta M P, Tian W, Datta S, Henderson J I and Kubiak C P 1996 *Phys. Rev.* B **53** R7626
[34] Ferretti A, Ruini A, Bussi G, Molinari E and Caldas M J 2004 *Phys. Rev.* B **60** 205205
[35] Wang Y, Liu J, Zhou J and Yang R 2013 *J. Phys. Chem.* C **117** 24716
[36] Tagani M B 2016 *J. Phys. D.: Appl. Phys.* **49** 125302
[37] de Oliveira Neto P H, da Silva Filho D A, Roncaratti L F, Acioli P H and e Silva G M 2016 *J. Phys. Chem.* A **120** 4923
[38] Zhang L, Keblinski P, Wang J S and Li B 2011 *Phys. Rev.* B **83** 064303
[39] Toshima N 2017 *Synth. Met.* **225** 3
[40] Leclerc M 2001 *J. Pol. Sci. A: Pol. Chem.* **39** 2867
[41] Giannozzi P *et al* 2009 *J. Phys.: Condens. Matter* **21** 395502
[42] Perdew J P, Burke K and Ernzerhof M 1996 *Phys. Rev. Lett.* **77** 3865
[43] Grimme S 2006 *J. Comput. Chem.* **27** 1787

[44] Vanderbilt D 1990 *Phys. Rev.* B **41** R7892
[45] WANT code by Ferretti A, Agapito L, Calzolari A and Buongiorno Nardelli M www.wannier-transport.org
[46] Datta S 1995 *Electronic Transport in Mesoscopic Systems* (Cambridge: Cambridge University Press)
[47] Calzolari A, Marzari N, Souza I and Buongiorno Nardelli M 2004 *Phys. Rev.* B **69** 035108
[48] Calzolari A, Jayasekera T, Kim K W and Buongiorno Nardelli M 2012 *J. Phys.: Condens. Matter* **24** 492204
[49] Agapito L A, Ferretti A, Calzolari A, Curtarolo S and Buongiorno Nardelli M 2013 *Phys. Rev.* B **88** 165127
[50] D'Amico P, Agapito L, Catellani A, Ruini A, Curtarolo S, Fornari M, Buongiorno Nardelli M and Calzolari A 2016 *Phys. Rev.* B **94** 165166
[51] Calzolari A and Buongiorno Nardelli M 2013 *Sci. Rep.* **3** 2999
[52] Gonze X and Lee C 1997 *Phys. Rev.* B **55** 10355
[53] Bruesch P and Fulde P 1986 *Phonons: Theory and Experiments* II (Berlin: Springer)
[54] Selvaganesh S V, Mathiyarasu J, Phani K and Yegnaraman V 2007 *Nanoscale Res. Lett.* **2** 546
[55] Quillard S, Louarn G, Lefrant S and Macdiarmid A G 1994 *Phys. Rev.* B **50** 12496
[56] Brenner P, Fleig L-M, Liu X, Welle A, Bräse S and Lemmer U 2015 *J. Pol. Sci. B: Pol. Phys.* **53** 1029
[57] Kim E J and Bredas J L 2008 *J. Am. Chem. Soc.* **130** 16880
[58] Libert J, Bredas J L and Epstein A J 1995 *Phys. Rev.* B **51** 5711
[59] Calzolari A, Vercelli B, Ruini A, Virgili T and Pasini M 2013 *J. Phys. Chem.* C **117** 26760
[60] Ramayya E B, Mauer L N, Davoody A H and Knezevic I 2012 *Phys. Rev.* B **86** 115328
[61] Mingo N and Yang L 2003 *Phys. Rev.* B **68** 245406
[62] Zoppi L, Calzolari A, Ruini A, Ferretti A and Caldas M J 2008 *Phys. Rev.* B **78** 165204
[63] Baroni S, de Gironcoli S, Dal Corso A and Giannozzi P 2001 *Rev. Mod. Phys.* **73** 515
[64] Ouyang Y and Guo J 2009 *Appl. Phys. Lett.* **94** 263107
[65] Grosso G and Pastori Parravicini G 2014 *Solid State Physics* 2nd edn (Amsterdam: Elsevier)
[66] Capaz R B and Caldas M J 2003 *Phys. Rev.* B **67** 205205
[67] Tang Y, Gibbs Z M, Agapito L A, Li G, Kim H-S, Buongiorno Nardelli S M and Snyder G J 2015 *Nat. Mater.* **14** 1223
[68] Dongmin Kang S and Snyder J G 2016 *Nat. Mater.* **16** 252
[69] Kim J, Jung J, Lee D and Joo J 2002 *Synth. Met.* **126** 311
[70] Bae E J, Kang Y H, Jang K-S and Cho S Y 2016 *Sci. Rep.* **6** 18805
[71] Faria G C, deAzevedo E R and von Seggern H 2013 *Macromolecules* **46** 7865
[72] Ranger M and Leclerc M 1999 *Macromolecules* **32** 3306
[73] Avery A D *et al* 2016 *Nat. Energy* **1** 16033
[74] Gu J W, Feng J J, Dang J, Li H L and Zhang Q Y 2014 *Adv. Mater. Res.* **893** 209